We are IntechOpen, the world's leading publisher of Open Access books Built by scientists, for scientists

4,800
Open access books available

122,000
International authors and editors

135M
Downloads

Our authors are among the

154
Countries delivered to

TOP 1%
most cited scientists

12.2%
Contributors from top 500 universities

WEB OF SCIENCE™

Selection of our books indexed in the Book Citation Index in Web of Science™ Core Collection (BKCI)

Interested in publishing with us?
Contact book.department@intechopen.com

Numbers displayed above are based on latest data collected.
For more information visit www.intechopen.com

9

Mechanism of Nano-Machining and Mechanical Behavior of Nanostructure

Jiaxuan Chen[1], Na Gong[1] and Yulan Tang[2]
[1]*Harbin Institute of Technology,*
[2]*Shenyang Jianzhu University*
China

1. Introduction

As the development of observing technology (such as the atomic force microscopy, AFM) and the increasing need of micro mechanical system in modern manufacturing industry, Nano-machining with machine tools and position-control techniques aim to produce high quality surfaces in terms to form accuracy, surface finish, surface integrity for optical mechanical and electronic components, has been a fundamental researching subject in ultra-precision machining area. Lots of researchers have shown extreme interest on the properties of nanoscale materials and the forming mechanism of nano-machining. Nowadays, although the AFM developed by Binnig et al [1] has been an effective instrument which is able to obtain directly the three-dimentional surface topography and can also been used to carry out the nanoindentation [2, 3] and nanocutting experiments[4, 5] in order to research on the mechanical properties and plastic deformation of materials. The details of plastic deformation, evolvement of defects and other important phenomenon in nano-machining processing are difficult to be observed clearly just by AFM. However, the molecular dynamics (MD) methods provides us a practical and effective way to research from the atomic perspective the removal mechanism, states of the stress and strain, the subsurface damaged layer, dislocation nucleation and propagation, surface friction and tool wear and so on [6-9]. In this chapter, we will introduce the method of applying MD simulation on the observing and analyzing of the nano-machining process to the readers in detail based on our researching results which have been published previously.

Meanwhile, as the basic components of micro mechanical system, nanostructures loaded show different mechanical response compared with macrostructures. Due to size effects, surface effects, and interface effects of nanostructures, properties of nanomaterials are enhanced, and nanoscale research has been an area of active research over the past decades. Many researchers use MD numerical simulation to investigate the physical mechanism of nanostructures by atomic motion in detail and have a rapid progress in recent years [10-21]. Most of those studies mainly concentrated on materials with free defects or artificial defects, however, as a matter of fact, a variety of defects can be generated in nano components during nanomachining process. Therefore, it is greatly important to have a suitable description of the material properties of nano-machined components. In this chapter, in order to find a better way to predict the material properties of microstructures, we established the model of real nanostructure with defect, and conduct the integrated MD

simulation of scratching and tension or scratching and shearing with the same specimen, respectively. So that, we will eventually find the regulation of real microstructures under different loading conditions and direct the design of nano-scale device.

2. Model and theory

With the development of the electronic industry, copper has been one of the important materials in many fields such as electrical interconnects, and in the past decade, which has been of significant interest to many researchers [22-27].In our simulations of nano-machining and nanostructures, we also considered the monocrystalline copper and pyramid rigid diamond as the workpiece and tool, respectively, as shown in Fig.1. The initial atomic configuration of the workpiece material is created from the face-centred cubic (FCC) copper lattice and the tool is tri-pyramid diamond tip with a rake angle of -60°. The atoms of workpiece are divided two parts. The upper part of workpiece is made of the 36 layers newtonial atoms and the atoms of surfaces are free, while the bottom of workpiece is made of the 4 layers boundary atoms and atoms are fixed in space at the process of scratching. The sizes of slab at x[1 0 0], y[0 1 0] and z[0 0 1] direction are 30, 17 and $18a_0$, where a_0 is the equilibrium lattice constant (for FCC Cu, a_0 = 362 nm).

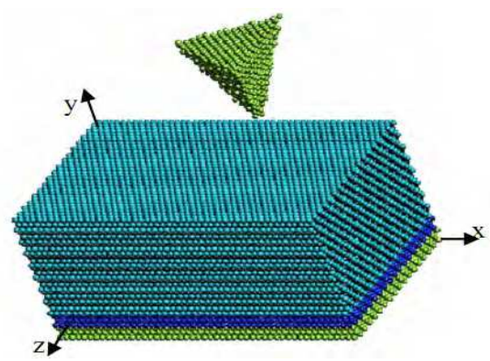

Fig. 1. MD simulation model of nano cutting on single crystal copper surface.

For the Cu–C interactions between workpiece atoms and tool atoms, the Morse potential is used. The Morse potential model [28-31] is adopted for the diamond atoms and the Cu atoms of the calculation process. The Morse potential is written as (1):

$$\mu r_{ij} = D[\exp(-2A(r_{ij} - r_0) - 2\exp(-A(r_{ij} - r_0)))] \tag{1}$$

where μr_{ij} is a pair potential energy function, D , A , r_0 and r_{ij} correspond to the cohesion energy, the elastic modulus, the atomic distance at equilibrium and the atomic distance between atom i and atom j, respectively.

The Cu–Cu interactions between workpiece atoms are described by the established embedded atom method (EAM) potential [32-36]. For the EAM potential, the total atomic potential energy of a system E is expressed as (2):

$$E = \sum_{i}^{N}[F(\rho_i) + \sum_{j>i}^{N} u(r_{ij})] \tag{2}$$

where E is the sum of the energy, $F(\rho_i)$ and $u(r_{ij})$ correspond to the sum of the embedding energy, the total potential energy. ρ_i is the host electron density at site induced by all other atoms in the system, which is given by (3):

$$\rho_i = \sum_j \phi(r_{ij}) \tag{3}$$

where $\phi(r_{ij})$ is the embedding function the electron density around an atom.

Usually, it is necessary to calculate stress of every atom in order to analyze the relations between the stress states of atoms and the onset of defects. The stress in the atomistic simulation mn on plane m and in the n-direction can be given by

$$\sigma_{mn} = \frac{1}{N_S}\sum_i [\frac{m_i v_i^m v_i^n}{v_i} + \frac{1}{2V_i}\sum_j F_{ij}\frac{r_{ij}^m r_{ij}^n}{r_{ij}}] \tag{4}$$

Where m_i is the mass of atom i, v_i is the volume assigned to atom i, N_S is the number of particles contained in region S, where S is defined as the region of atomic interaction, r_{ij} is the distance between atoms i and j, and r_{ij}^m and r_{ij}^n are two components of the vector from atom i to j.

The temperature of the entire system was maintained at 293 K with a Nos'e–Hoover thermostat [37, 38], and the half step frog leap algorithm was used for time integration of the atomic coordinates. Through preset the different simulation conditions, such as the cutting face and direction, the depth of nano-cutting, scratching speed, rank angle and so on, we are able to study in depth the removing mechanism of material, state of stress and strain, forming and evolvement of defects, fluctuating of cutting force and other important and interesting processing phenomenon, during the course of nano-machining or nanostructure loading.

3. Mechanism of nano-metric cutting

The workpiece is relaxed to minimum energy before scratched. At the initial stage of scratching process, some atoms of workpiece leave workpiece to be absorbed on the fronter surface of tool under the cutting and attracting action of tool, material ahead and beneath the cutting tool is deformed during scratching, which is similar to the conventional cutting process. With the pas- sage of tool, more and more atoms of workpiece begin to climb along the frontier surface of tool under the shearing and attracting force of tool, and stack the frontier surface on of tool, which is the primeval stage of chip forming as shown in Figure 2 below [39]. In the whole process of scratching, the lattice of the workpiece is deformed as by buckling and compressing due to plowing of the tool, and those atoms near the tool, especially that ahead the tool are affected by the stress from the motion of tool and obtain the higher energy .The atoms with high migration energy leave its initial position, and accomplish the workpiece removed by the attraction and compression of the tool.

Due to shearing and compressing action of tool, atoms of workpiece are applied forceful shear and nor-mal stress. When those stresses get to some extents, dislocations begin to

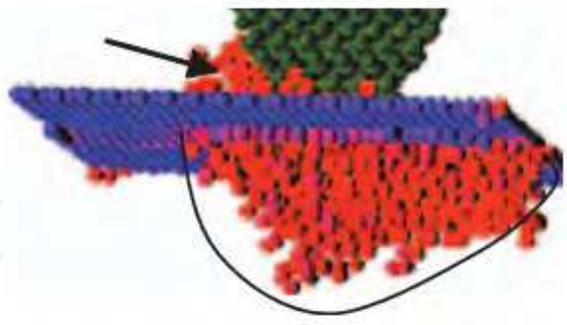

Fig. 2. The chip deforming of single crystal copper scratched on (010) plane by triangular-based pyramid tool with -60°rank angle. Arrow shows chip deforming.

appear. At the initial scratching stage dislocations are driven and propagate only in surface and subsurface of workpiece, and expand to another free surface along the [−101], [10–1] direction on the surface. With progress of the cutting edge, the numbers of pile-up atoms on surface of tool increase obviously, the numbers of atoms which play the cutting role increase accordingly, atoms of workpiece are applied to the more forceful stress and the range of atoms affected is wider, some dislocations are driven by shearing stress and normal stress, and begin to propagate downwards on {111} plane in workpiece. The deformed regions beneath machined surface of workpiece are smaller than that beneath surface being machined, and show the elastic restore to some extents, as shown in Figure 3.

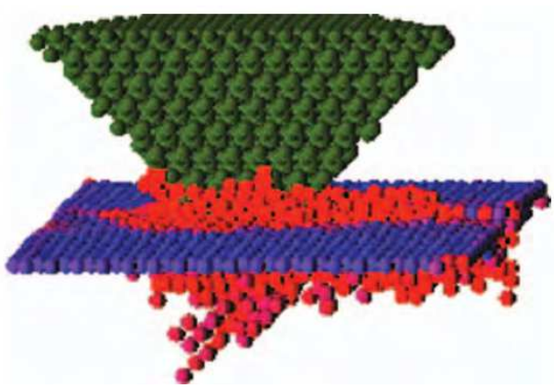

Fig. 3. Triangular-based pyramid tool with -45°rake angle scratching monocrystal copper {010} plane, dislocations propogate downwards on {111} plane in workpiece.

Compared with the condition of -60°rake angle, we can see that the deformed region beneath tool is broadened, and the deformed region beneath machined surface of workpiece is also broadened with the increasing scratching depths and rake angle. As a result, the numbers of defects in workpiece increase under the big scratching depths, while the order degree of latticedecreases, especially for the distribution of short–range order, the atomic numbers of regular position decrease, which are also shown in Figure 4.

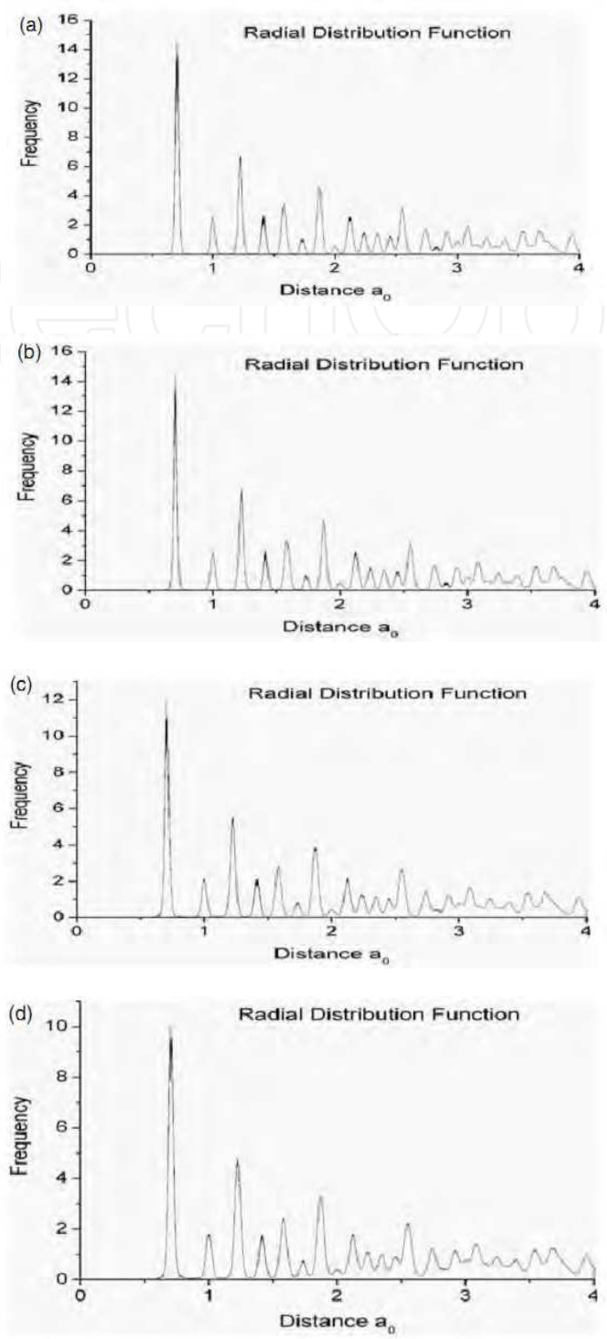

Fig. 4. The order degree of atoms in workpiece after triangular-based pyramid tool with −45°rake angle scratch monocrystal copper {010} plane with scratching depths 0.5, 1, 2, 3 a_0.

In the scratching process, with increasing depths of scratching, the numbers of atoms what play the cutting role are augmented, and the number of removal atoms also increase, which need larger cutting force, the cutting force for tool with rake angle −30° is larger than that for tool with rake angle −45°at the same scratching depths, the curves of scratching force for different scratching depths and rake angle are shown in Figure 5 below.

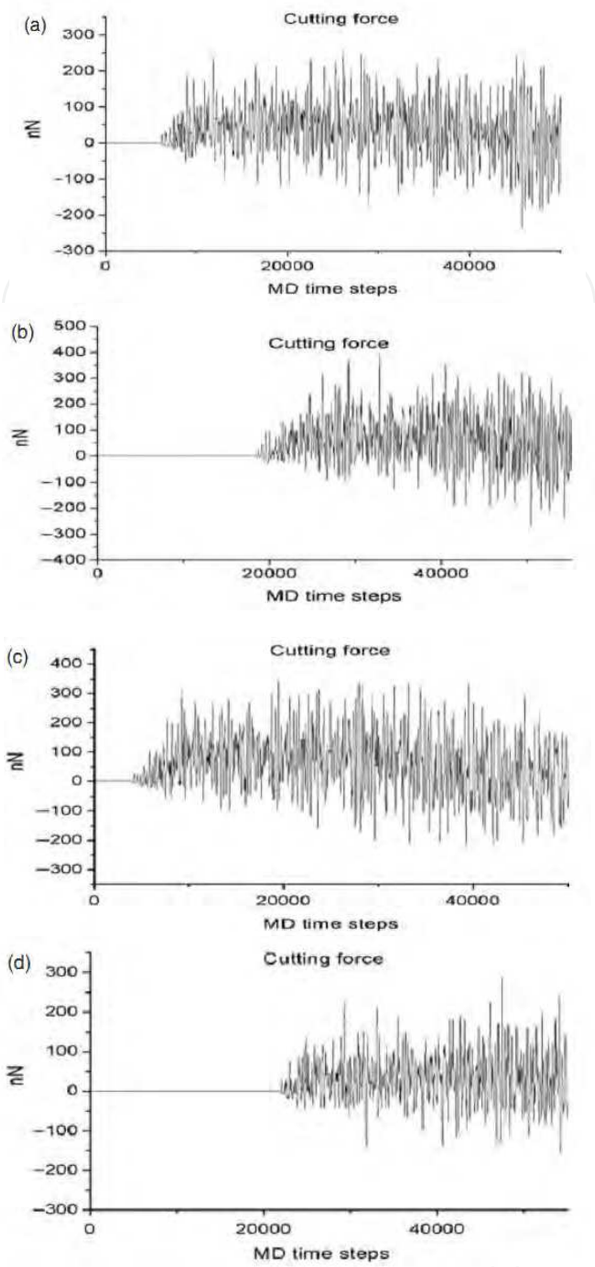

Fig. 5. The scratching force of triangular-based pyramid tool scratching monocrystal copper {010} plane under scratching depths1, 3 a_0: (a–b) −30°rake angle, (c–d) −45°rake angle.

With increasing scratching depths, atoms of workpiece receive the more forceful action of shearing and compression, the effected range of atoms in workpiece are also broaden, though some effected atoms restore their usual position, there are still more defects' atoms to exist in workpiece after tool scratch the workpiece. At the same time, there exists the higher residual stress in workpiece after tool withdraws the workpiece as shown in Figure 6.Though residual stress can decrease by anneal process,the level of residual stress in subsurface of workpiece with the increasing scratching depths enhance accordingly, the

level of residual stress in subsurface of workpiece that scratched by tool with rake angle −45˚is higher than that rake angle −30˚.

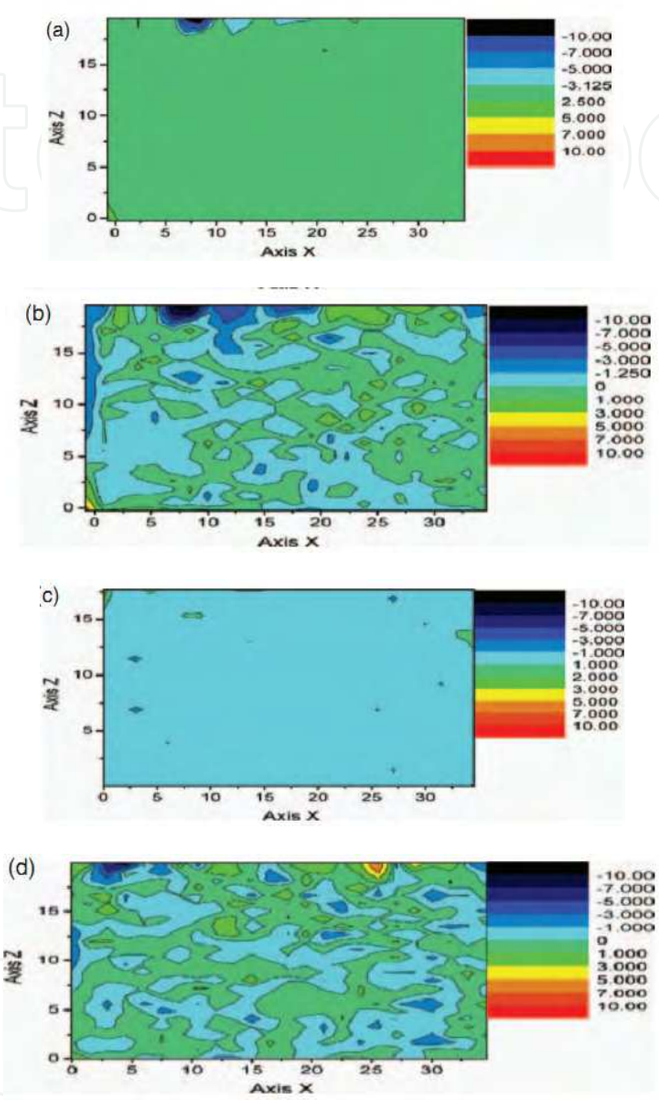

Fig. 6. The shear stress distribution of atoms in subsurface with differ-ent rake angles and scratching depths after relaxation: (a–b)-scratching depths 0.5, 3 a_0 for −45˚rake angle; (c–d)-scratching depths 0.5, 3 a_0 for −30˚rake angle.

The workpiece crystal orientations also have important effects on defects evolvement, as shown in Fig.7. When the AFM diamond tip scratches the surface of single crystal copper as shown in Fig. 7(a), it can be seen that dislocation is prone to nucleate ahead the tool, and those dislocations glide in the [101] direction as the effects of the edge of the AFM diamond tip. The Fig. 7(b) shows the case of (110) plane of single crystal copper. From the Fig. 7(b), it is found that dislocations glide in the [-101] direction. For the case of (111) plane of single

crystal copper, the dislocations seem to propagate the dislocations propagate at 30o to the cutting direction at the top surface, and dislocations glide in the [1-10] direction and [01-1] direction as shown in Fig. 7(c) [40].

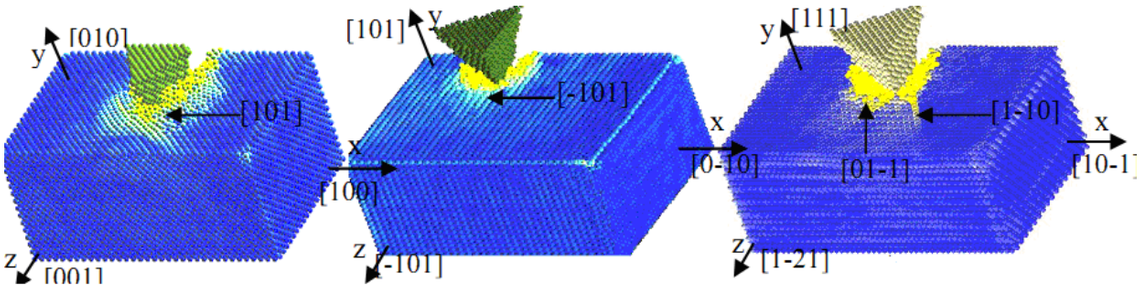

(a) (b) (c)

Fig. 7. The atom snaps of nano-cutting single copper on different orientation: (a) (100) orientation, (b) (110) orientation and (111) orientation.

Fig.8 shows the variation curve of fluctuating cutting force under different orientation and the same cutting depths. From Fig.8, we can see that the nucleation and propagation of dislocations results in the release of the accumulated cutting energy, which corresponds to the temporary drop of the cutting force due to the complex local motions of the dislocations. It also can be seen from the curves that the cutting force of the steady state from (111) orientation is the biggest, that from (110) orientation is the lowest.

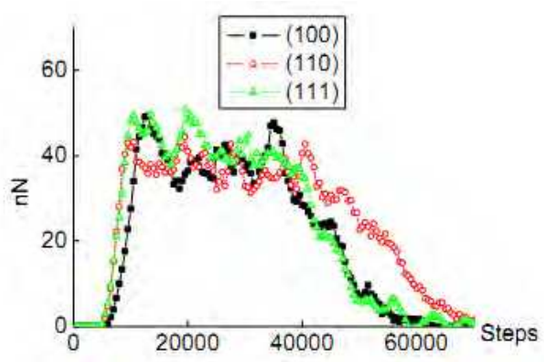

Fig. 8. Effect of crystal orientation on cutting force.

We also find that the scratching speed has important effects on dislocations evolvement. Fig.9 shows the relationship of the numbers of defects and the scratching speed. From Fig.9 we can see that dislocations can propagate succeeding under the low scratching speed. We also can see that the order of the atoms of workpiece under high scratching speed is better than low scratching; the numbers of defects inside workpiece with high scratching speed are low corresponding to the low scratching.

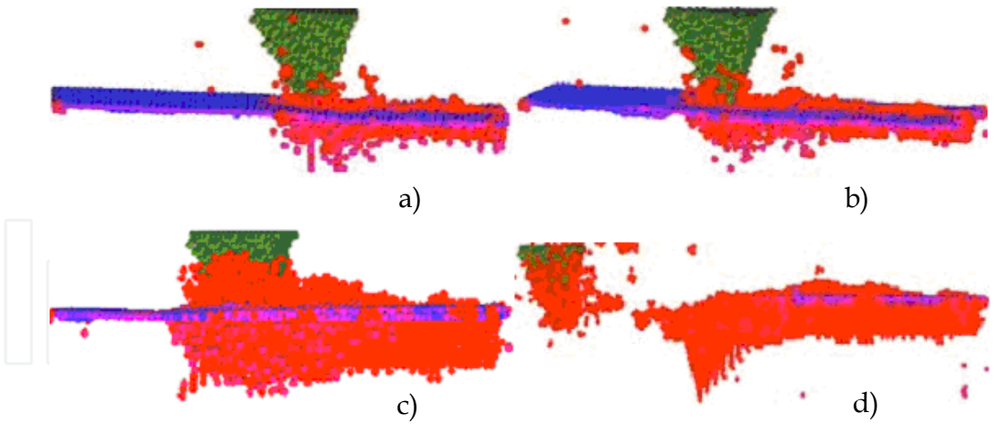

Fig. 9. The picture a1 and a2 indicate the effects of dislocations evolvement under the scratching speed 360m/s. The picture b1 and b2 under the scratching speed 180m/s.

4. Mechanical behavior of nanostructure

The nanostructure with no defects or artificial defects are not suitable to simulate the material properties of practical nanostructure. in this part, we introduce an integrated MD simulation method, in order to study the mechanical properties of nanostructure with practical processing defects. We consider the nanostructure scratched by diamond tip under the machining conditions of different scratching depth of different scratching lattice plane or direction, just like we have described above, as the practical processing defects, then, apply tension or shearing force on such nanostructure to observe their physical and mechanical behavior.

4.1 Scratching and tension

The models we established are shown in figure 10, we also introduce the ideal nanostructure with no defects for comparing. For ideal copper specimen, as shown in Fig.10 (a), the sizes of slab at X[100], Y [010], and Z[001] direction are $12a_0$, $17a_0$, and 20 a_0, respectively, where a0 is the equilibrium lattice constant (for fcc Cu, a_0=0.362 nm); For machined specimen, as shown in Fig 10 (b) and (c), which can be obtained as followed: a tri-pyramid diamond tool scratches an ideal fcc copper slab on the (010) plane along [001] and [100] directions, Newton atoms layers are and the states of these atoms should be kept, the two ends of Newton atoms are picked up $2a_0$ length along axis Z [001] and Z [00-1] direction to become the boundary layer atoms respectively [41].

Before simulation, the ideal specimen is relaxed for 10000 MD steps for minimizing energy. After that, double tensile loads are applied to the two ends of specimen. At the initial stage, though the atoms of specimen begin to deviate from their positions, the configurations of lattice don't change, as shown in Fig 11 (a) and 11(b), which is corresponding to elastic stage in stress-strain curve, as shown in Fig 12 (a). During tensile process, when normal stress σ_{zz} is up to the first peak point, defects such as dislocations begin to occur and propagate along different {111} planes under tensile loads due to the smallest Burgers vector existing in the [110] close-packed directions for fcc crystal structures, making it most energetically favorable to reconstruct along this plane. Because of the motion of dislocations, the higher

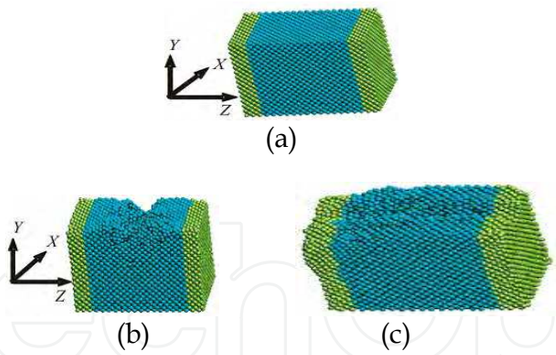

Fig. 10. (a) Model for ideal specimen; (b) Model for mahined specimen along [001] direction; (c) Model for machined specimen along [100] direction.

stress is released and normal stress σ_{zz} begins to decrease. As the increasing of defects, which hinder the motion of dislocation freely, and result in work-harden formation. It is necessary to obtain forceful force to drive the motion of dislocations, which exhibits that normal stress σ_{zz} increase secondly in stress-strain curve. After the second yield, ideal specimen begin to neck under tensile loads, and corresponding to the stress-strain curve begin to decrease quickly, and occur to rupture at the neck region firstly, as shown in Fig.13 (a)and(b). So the deformation of nanostructure experiences next process: elastic stage, first yielding and work-harden stage, second yielding and full plastic stage, rupture [42].

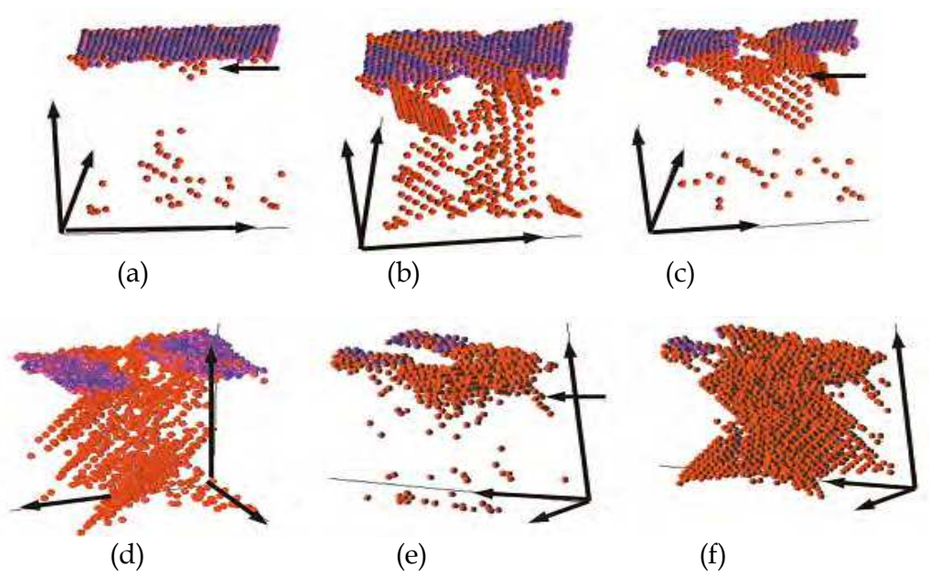

Fig. 11. (a) and (b) ideal specimen at strain 0.066 and 0.089,and atoms are shown for slip index 0.20, respectively, and tensile speed is 7.6 m/s; (c) and (d) scratched specimen with groove for depth $1a_0$ along $[\bar{1}00]$ direction at strain 0.0615 and 0.075 respectively, and atoms are shown for slip index >0.20, and tensile speed is 3.6 m/s; (e) and (f) scratched specimen with groove for $2a_0$ depth along $[00\bar{1}]$ direction at strain 0.0486 and 0.077 respectively, and atoms are shown for slip index >0.20, and tensile speed is 3.6 m/s arrows denote dislocations.

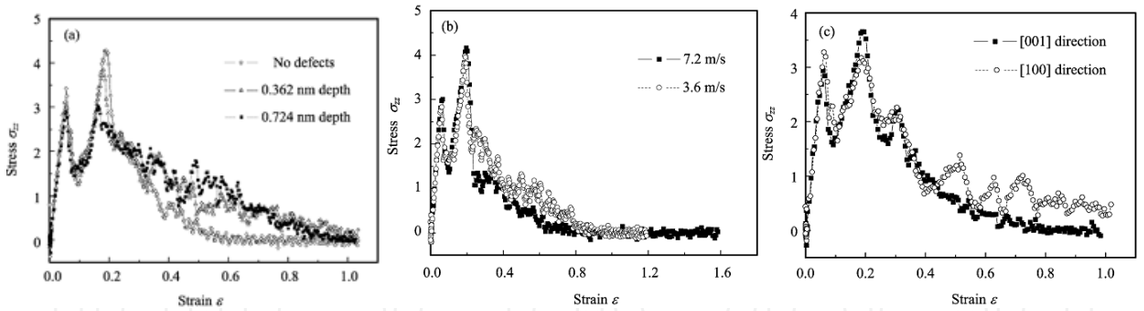

(a) (b) (c)

Fig. 12. (a) Specimen with scratched groove along $[00\bar{1}]$ direction for tensile speed 3.6 m/s; (b) Specimen with scratched groove at $1a_0$ depth along $[00\bar{1}]$ direction; (c) Spec-imen with scratched groove at $2a_0$ depth.

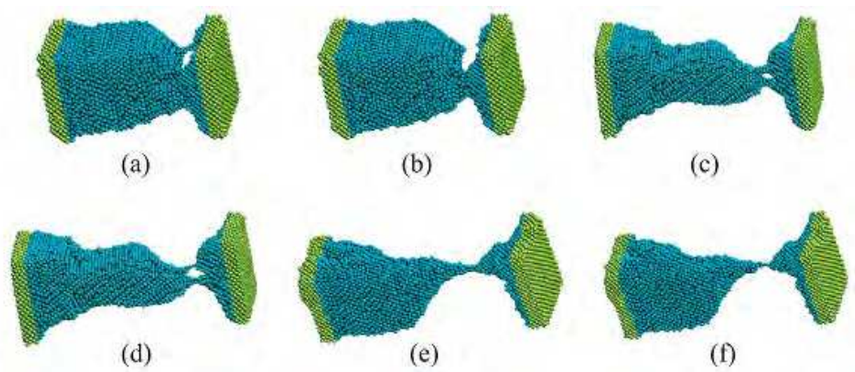

Fig. 13. (a) and (b) ideal specimen at strain 0.437 and 0.495 for tensile speed 3.6 m/s; (c) and (d) specimen with scratched groove along $[00\bar{1}]$ direction for $2a_0$ depth, strain 1.068 and 1.071; specimen with scratched groove along $[00\bar{1}]$ direction for $1a_0$ depth, strain 1.23 and 1.28, tensile speed 3.6 m/s.

For scratched specimen case, the process of relaxation and force applying are in the same way with the ideal specimen case. The stress-strain curves are shown in Fig.12 (a)-(c). From Fig.12 (a)-(c), we can see that specimens machined also exhibit the initial stage of nearly elastic response, then two peaks, work-hardening stage and rapture at last, which is also the same as the specimen with on defects. From Fig.12(a), it can be seen that the first yielding and second yielding normal stress decrease as the depths of scratched groove on surface of specimen increase. From Fig.12 (b), it can be seen the numerical value of the first and the second yielding stress for specimen with scratched groove of $1a_0$ depth under higher tensile speed are higher than lower tensile speed. It shows that yielding strength of specimen increase with increasing tensile speed. From Fig.12(c), we can see that when the direction of scratched groove is consistent with the extension direction, under the same groove of depth and tensile speed, the second yielding stress is higher than the direction of groove is in perpendicular direction of extension.

For machined specimen, we also notice that dislocations prone to nucleate not only from surface and corner of specimen just as the ideal specimen case, but also from groove, in particular from the position of ends of groove, and then dislocations begin to propagate

along different (111) planes, as shown in Fig.11 (c)-(g). For the case that the direction of scratched groove is in the perpendicular direction of extension, dislocations prone to nucleate from the position that tool withdraw specimen firstly.

4.2 Scratching and shearing

Another usual loading condition is shearing for nanostructure. Here, following the method we have described above, we begin to study the mechanical behavior of practical nanostructure under the shearing load. The model established is shown as Fig.14. Through setting the different simulation conditions, such as the model size and the depth of groove , we can research in depth the affecting regulation of these elements on the mechanical and physical behavior.

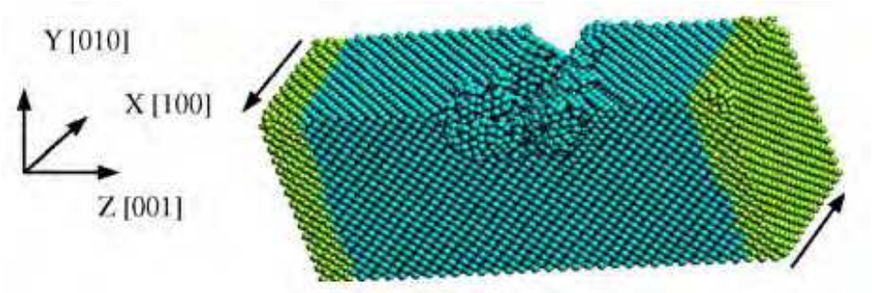

Fig. 14. Shearing simulation model for scratched specimen with arrows denoting directions of loading.

The stress-strain curves generated from the simulations of shearing with specimens without defect and specimen with groove at scratch depths of 0.5, 1, 2, 3, $5a_0$ are as shown in Fig. 15. From Fig.15 we can see that the deformation of specimen experience an elastic response at the initial stages, and then elastic–plastic stage near PSS (peak shear stress), and total plastic stage after PSS. From the moment when plastic yielding occurs in the specimen to the moment when the specimen plastically fails under continuous shear loads, shear stress τ_{xz} drops firstly, and then remains steady for a certain length of time before another decline starts, and the stress–strain curves decrease again, and are shown in zigzag changes, and a total failure occurs at the end of the second decline. Normal stress σ_{xx} fluctuates around zero firstly, and then it begins to gradually increase when the nanostructures begin to yield. When normal stress σ_{xx} goes up to the same level as shear stress τ_{xz}, normal stress σ_{xx} begins to decrease with shear stress τ_{xz}. It can be seen from the stress–strain curves shown in Fig. 15a and b that shear stress τ_{xz} plays a leading role in the initial stage of shearing process. The contribution of normal stress σ_{xx} begins to increase when the yielding starts, and normal stress σ_{xx} and shear stress τ_{xz} play the same role for plastic deformation of specimen.

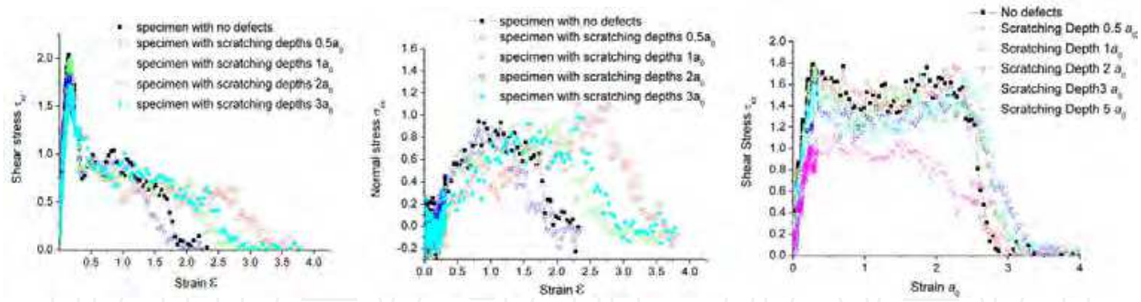

(a) (b) (c)

Fig. 15. (a) And (b) Normal stress σ_{xx} and shear stress τ_{xz} stress–strain curves for specimen at size 12-15-20a_0 without defects and scratching depths of 0.5, 1, 2 and 3a_0 and (c) shear stress–strain for specimen at sizes 12-15-35 a_0 without defects and at scratching depths 0.5, 1, 2, 3 and 5a_0.

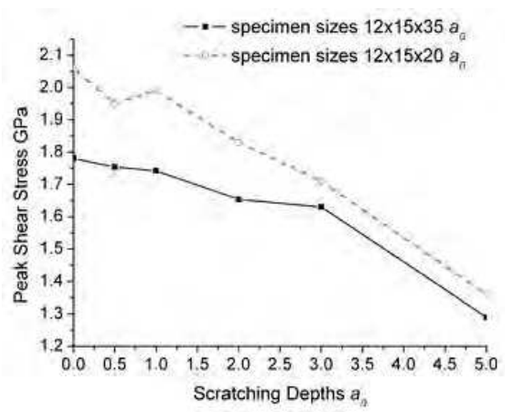

Fig. 16. Peak shear stress τ_{xz} obtained with of different sizes at different scratching depths specimens

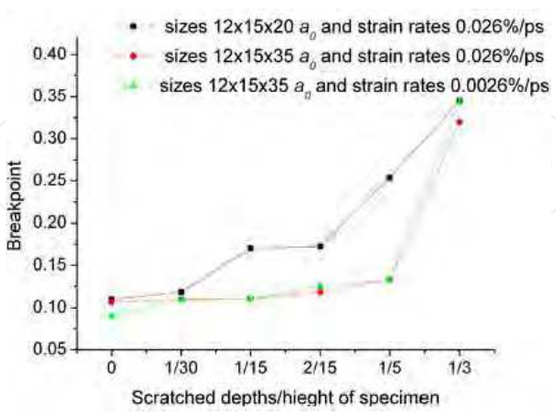

Fig. 17. The breakpoint of specimen under high-speed shear loads.

PSS of specimen for different sizes and different depths are shown in Fig. 15. From Fig. 15, it can be seen that PSS decreases with the increasing depths of scratching and an ideal specimen is the highest. This is mainly because of that dislocations are likely to nucleate in

the specimen with many defects on nano scale, which results in the decreasing of shear intensity. It also can be seen from Fig. 15 that the yield stress of scratched specimen also decreases with the increasing specimen size. The yield stress is observed to decrease with the increasing specimen size, which is due to the enhanced opportunities for dislocation motion to occur at a larger size. For small specimen sizes, PSS increases at the same scratch depths, which show size effect (namely the scale dependence, that the size and quantity of defects inside the nanostructure decrease and the intensity improve when its scale becomes smaller and smaller, and thus the nanostructure will show different mechanical properties compared with body material)

For an ideal specimen or a specimen with shallow scratch depths, the stress gradients is flat near the groove, the dislocations resulting from the stress field at the corner are the main sources of plastic deformation, and the breakpoint of failure is close to the either end of the specimen. With the increasing scratch depths, the gradient of stress is steep near the groove, are likely to overtake the bafflement to cause the movement of dislocations, and thus the stress gradients near the corners and/or the groove induce the dislocations to determine the yielding point. In this way, the yield plastic deformation is likely to occur near the groove, and the breakpoint of failure is close to the groove of the specimen. Fig.17 shows the breakpoints of specimen under shear loads. It can be seen from Fig. 17 that the breakpoint is close gradually to the groove as the depth of groove increases. At the same scratched depths, the breakpoint is closer to the groove for a small specimen. It is noted that the breakpoint of specimen can be determined by groove when the ratio of the depths of groove to the height of specimen is up to one third (scratched depths $5a_0$) regardless of size and strain rates [36].

When the specimen is continuously subjected to the shear load, the specimen begins to yield and break down. The snapshots of the rupture processes of specimen are as shown in Fig. 18. From Fig.18 we can see that the formations of rupture of nanostructure are that the development of vacant clusters in the neck region which causes the rupture of specimen, or gradual thinning of theneck region of the scratched specimen into a single chain of atoms.

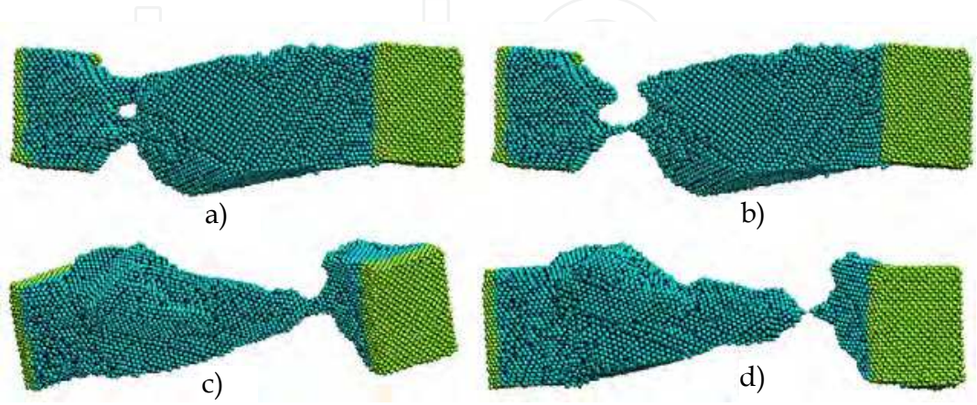

Fig. 18. (a) and (b) the formation of rupture of specimen with no defects for shear simulation, (c) and (d) that of specimen with scratching depths of $5a_0$.

5. Conclusion

Because of the smaller size of the nanostructure and the lack of related instrument, the traditional experimental method is not suitable to study the mechanical behavior of nanostructure. However, lots of researching work proves that the MD simulation method is a feasible method to study the mechanical and physical properties and plastic deformation of materials in nanoscale. based on the simulating results we provide above, we find that the removal mechanism of material, and states of the stress and strain of structure in nanoscale show obvious differences compared with macrostructures, such as the size effects, surface effects, and interface effects, two yield peaks et al. and the defects induced by machining play an important role during the dislocations moving and material yielding, and lead to the rupture of nanostructure loaded at last. MD simulation method is able to make the researchers to observe directly and clearly this phenomenon and find the hiding regulations in micro processing. The deep and wide study will improve the development of modern electrical industry and the whole manufacturing industry in the future.

6. Acknowledgment

We would like to thank the National Science Fund for Distinguished Young Scholars of China (50925521), the Natural Science Foundation of China (51075092), the Natural Science Foundation of Heilongjiang Province in China (E200903) and China Postdoctoral Science Foundation (20100471020), and Harbin Innovative Talents Fund (2011RFQXG017) for their financial supports.

7. References

[1] G. Binnig, C.F. Quate, and C. Gerber, Physics Review Letter 56 (1986) 930.
[2] S.G. Corcoran, R.J. Colton, E.T. Lilleodden, and W.W. Gerberich, Physical Review B 55 (1997) 16057.
[3] R. Smith, D. Christopher, S. D. Kenny, A. Richter, and B. Wolf, Physical Review B 67 (2003) 245405.
[4] T. Sumomogi, T. Endo, and K. Kuwahara, Journal of Vacuum Science and Technology B 12 (1994) 1876.
[5] Y.D. Yan, T. Sun, Y.C. Liang, and S. Dong, International Journal of Machine Tools & Manufacture 47 (2007) 1651.
A. Gannepalli, and S. K. Mallapragada, Physics Review B, 66 (2002) 104103.
[6] R Komanduri, N Chandrasekaran, and L.M Raff, Physical Review B, 61 (2000) 14007.
[7] K. Cheng, X. Luo, R. Ward, and R. Holt, Wear, 255 (2003) 1427.
[8] S. Shimada, SPIE, 2576 (1995) 396.
[9] R. Komanduri, N. Chandrasekaran, and L. M. Raff, International Journal of Mechanical Sciences, 43 (2001) 2237.
[10] H. A. Wu, European Journal of Mechanics - A/Solids, 25 (2006) 370.
[11] Y. Champion, C. Langlois, G. M. Sandrine, P. Langlois, J. L. Bonnentien, and M. J. Hytch, Science 300 (2003) 1357.
[12] S. J. A. Koh, H. P. Lee, C. Lu, and Q. H. Cheng, Physical Review B 72 (2005) 085414.
[13] S. P. Ju, J. S. Lin, and W. J. Lee, Nanotechnology 15 (2004) 1221.
[14] J. W. Kan and H. J. Hwang, Nanotechnology 13 (2002) 524.

[15] S. A. Kotrechko, A. V. Filatov, and A. V. Ovsjan-nikov, Theoretical and Applied Fracture Mechanics 45 (2006) 92.
[16] D. S. Xu, R. Yang, J. Li, J. P. Chang, H. Wang, D. Li,and S. Yip, Computational Materials Science, 36 (2006) 60.
[17] F. Golovnev, E. I. Golovneva, and V. M. Fomin, Computational Materials Science, 36 (2006) 176.
[18] H. S. Park and J. A. Zimmerman, Physical Review B 72 (2005) 054106.
[19] K. A. Ifat, R. C. Sidney, G. Konstantin, I. Viktoria, H.Thomas, S. Gotthard, W. Inna, H. D. Wagner, and T.Reshef, Proceedings of the National Academy of Sciences, 103 (2006) 523.
[20] P. Heino, H. Ha, K. Kinen, and K. Kask, Physical Review B 58 (1998) 641.
[21] Y. W. Zhang, T. C. Wang, and Q. H. Tang, Journal of Applied Physics, 77 (1995) 2393.
[22] S. Shimada, International Journal Japan Society Precision Engineering, 29 (1995) 283.
[23] S.Shimada, SPIE 2576 (1995) 396.
[24] Y. Y. Ye, R. Biswas, J. R. Morris, A. Bastawros, and A. Chandra, Nanotechnology 14 (2003) 390.
[25] P. Heino, H. Ha. K. kinen, and K. Kask, Physical Review B, 58 (1998) 641.
[26] Win. Jin. Chang, Microelectronic Engineering, 65 (2003) 239.
[27] R. Komanduri, M. Lee, and L.M. Raff, International Journal of Machine Tools & Manufacture, 44 (2004) 1115.
[28] Komanduri, R., Chandrasekaran, N. and Raff, L.M. Philosophical Magazine B, 79 (1999) 955.
[29] Komanduri, R., Chandrasekaran, N. and Raff, L.M. Physical Review B, 6 (2000) 14007.
[30] Komanduri, R., Chandrasekaran, N. and Raff, L.M. Wear, 240 (2000)113.
[31] M.S. Daw, and M.I. Baskes, Physical Review Letter, 50 (1983) 1285.
[32] M.S. Daw, and M.I. Baskes, Physical Review B, 29 (1984) 6443.
[33] R.A. Johnson, Physical Review B, 37 (1988) 3924.
[34] R.A. Johnson, Physical Review B, 39 (1989) 12554.
[35] Y.C. Liang, J.X. Chen, M.J. Chen, Y.L. Tang and Q.S. Bai, Computational Materials Science, 43 (2008) 1130.
[36] S.Nose, Journal Chemical. Physics, 81 (1984) 551.
[37] W.G.Hoover, Physical Review A, 31 (1985) 1695.
[38] J.X. Chen, Y.C. Liang, Q.S. Bai, Y.L. Tang. M.J. Chen. Journal of Computational and Theoretical Nanoscience, 5 (2008) 1485
[39] JX. Chen, Y.C. Liang, L.Q. Wang, M.J. Chen, Z. Tong, W.Q. Chen, Proceedings of SPIE, 7655 (2010) 76550J
[40] Y.C. Liang, J.X. Chen, M.J. Chen , Y.L. Tang and Q.S. Bai, Chinese Journal of Chemical Physics, 20 (2007) 649
[41] Y.C. Liang, J.X. Chen, Q.S. Bai, Y.L. Tang, M.J. Chen. Acta Metallurgica Sinica, 44 (2008) 119

Materials Science and Technology
Edited by Prof. Sabar Hutagalung

ISBN 978-953-51-0193-2
Hard cover, 324 pages
Publisher InTech
Published online 07, March, 2012
Published in print edition March, 2012

Materials are important to mankind because of the benefits that can be derived from the manipulation of their properties, for example electrical conductivity, dielectric constant, magnetization, optical transmittance, strength and toughness. Materials science is a broad field and can be considered to be an interdisciplinary area. Included within it are the studies of the structure and properties of any material, the creation of new types of materials, and the manipulation of a material's properties to suit the needs of a specific application. The contributors of the chapters in this book have various areas of expertise. therefore this book is interdisciplinary and is written for readers with backgrounds in physical science. The book consists of fourteen chapters that have been divided into four sections. Section one includes five chapters on advanced materials and processing. Section two includes two chapters on bio-materials which deal with the preparation and modification of new types of bio-materials. Section three consists of three chapters on nanomaterials, specifically the study of carbon nanotubes, nano-machining, and nanoparticles. Section four includes four chapters on optical materials.

InTech Europe
University Campus STeP Ri
Slavka Krautzeka 83/A
51000 Rijeka, Croatia
Phone: +385 (51) 770 447
Fax: +385 (51) 686 166
www.intechopen.com

InTech China
Unit 405, Office Block, Hotel Equatorial Shanghai
No.65, Yan An Road (West), Shanghai, 200040, China
中国上海市延安西路65号上海国际贵都大饭店办公楼405单元
Phone: +86-21-62489820
Fax: +86-21-62489821

IntechOpen